



Unsteady targeted particle delivery in three-dimensional tortuous cerebral artery

Pawan Kumar Pandey¹  · Malay Kumar Das¹

Published online: 7 May 2020
© Indian Institute of Technology Madras 2020

Abstract The present work investigates the complexities of unsteady targeted particle delivery in tortuous cerebral artery with three-dimensional twists and bends. Blood flow is modeled to mimic realistic pulsatile flow conditions along with its shear thinning behavior. One-way coupling is used to model particle flow. Dynamic particle release map (DPRM) for the targeted site, saccular aneurysm sac present in the artery, is determined on a chosen lumen cross section. Temporal variations in DPRM are analyzed and preferable catheter injection position and particle release pattern are recommended for minimum systemic toxicity.

Keywords Hemodynamics · Particle trajectory · Catheter · Dynamic particle release map (DPRM)

Additional notations

$\langle \rangle$ Phase average
 $\langle \rangle^f$ Intrinsic phase average

List of symbols

\mathbf{V} Velocity vector (m/s)
 V Velocity magnitude (m/s)
 P Pressure (Pa)
 X Spatial variable (m)
 d Diameter (m)
 μ Dynamic viscosity (Pa s)
 $\dot{\gamma}$ Shear (s^{-1})
 ε Porosity
 K Permeability

Subscripts

f Blood
 ij Indices of tensor
 p Particle

1 Introduction

Many medical complications require direct drug delivery at the intervention sites. Direct tumor targeting and live thrombus dissolution come under this treatment approach. Drug particles, under controlled conditions, are injected through the catheter at some upstream locations [1, 2]. These drug particles then flow with bloodstream, and a fraction of injected particles reach the targeted diseased site. The primary concern in this approach is to reduce the count of drug particles missing the targeted sites. Missed drug particles act on unwanted sites and cause systemic toxicity [3]. A thorough investigation of the effects of hemodynamic complexities, particle characteristics and catheter injection conditions (position and intrusion time) is required to ensure the zero systemic toxicity.

Several complexities can arise while modeling drug particle transport through the blood. It is a complex fluid with many deformable biological cells suspended in plasma. Because of these cells blood exhibits shear thinning behavior in arteries and arterioles [4], pulsatile flow and tortuous arteries make flow even more complex. These factors cause high unpredictability of injection sites efficiency. Under these conditions, medical professionals, performing targeted delivery of drug particles, require a helping hand from a computational approach [2]. Works in [1, 2] report the particle release map (PRM) for tumor targeting. Particle release map for steady flow and dynamic

✉ Malay Kumar Das
mkdas@iitk.ac.in

¹ Department of Mechanical Engineering, Indian Institute of Technology Kanpur, Kanpur, India

particle release map (DPRM) for unsteady flow are the contour map of the initial injection position of particles getting successfully delivered at the targeted site.

Emboli transport and tracing its atherogenic root site is also the problem of inverse nature and similar challenges. This kind of work in the literature can also help us to better understand particle dynamics while flowing with blood. Works in [5–7] try to understand different aspects of the emboli trajectory and its interaction with hemodynamics. Large emboli particles show a preferential behavior for arteries with a larger diameter [5]. As intuition would have

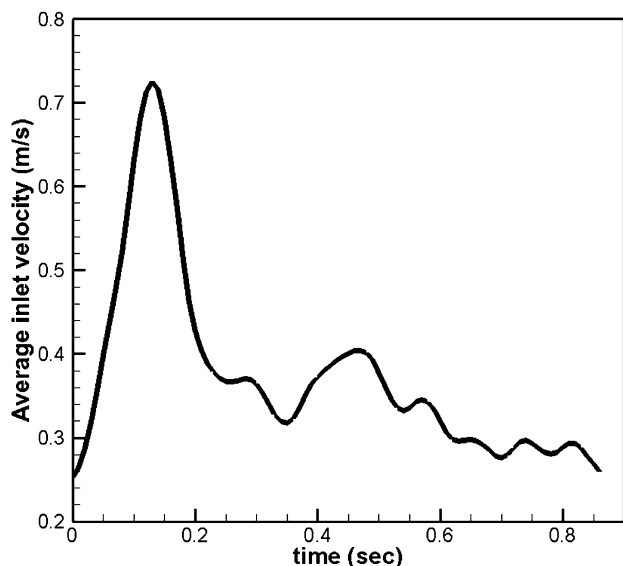


Fig. 1 Physiological velocity waveform in cerebral artery

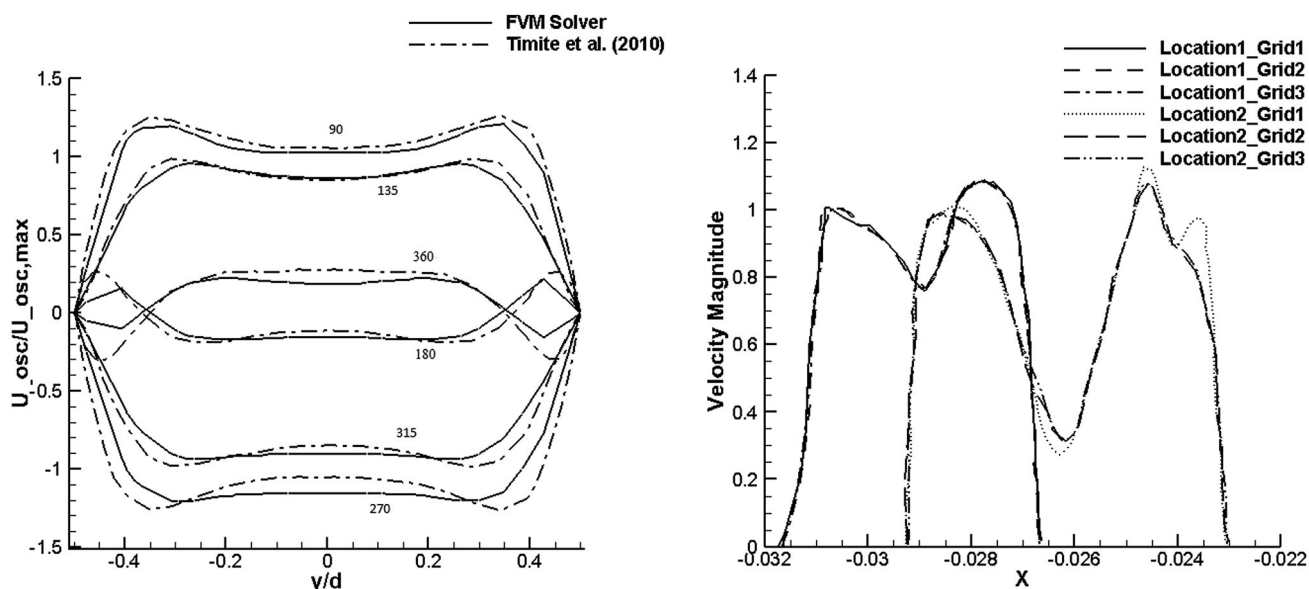


Fig. 2 Normalized velocity profiles compared with the results of Timite et al. in [13]. Profiles are shown for phase angle of 90°, 135°, 180°, 270°, 315° and 360°. Plot of grid independence study is shown on the right

suggested [8] proved that particle trajectories also depend on the particle size, density and velocity. Larger particles with larger velocity tend to exhibit a more tortuous trajectory compared to particles with lesser momentum [9]. This phenomenon causes the preferential flow of particles in the daughter vessel. Upstream vessel anatomy can affect particle aggregation/deposition behavior in multiple level downstream daughter vessels too [7].

Size, shape, and density are primary characteristics of particles that affect the adhesion with the endothelium layer of vessels. Higher-density particles show higher margination toward the wall reducing the possibility of a capillary block. Non-spherical particles show better adhesive behavior but their use in practice is limited due to synthesis difficulties [8].

Several works in the literature present targeted drug delivery studies for tumor targeting. We believe the present study is the first of its kind to explore the possible targeted drug delivery for peripheral arterial disease (aneurysm in the present case). Delivery of hemostatic agents inside the bleeding aneurysm can be a preferable treatment option if its side effects like deep vein thrombosis could be eliminated. Targeted delivery can reduce the chances of thrombus formation due to target missed particles. To determine DPRMs and optimal release strategy is the primary objective of present work. With the aid of determined DPRMs, we calculate the maximum catheter size that can be used with zero systemic toxicity ensured. We present four different particle release strategies with varying catheter intrusion time. Investigation of the mass effects of

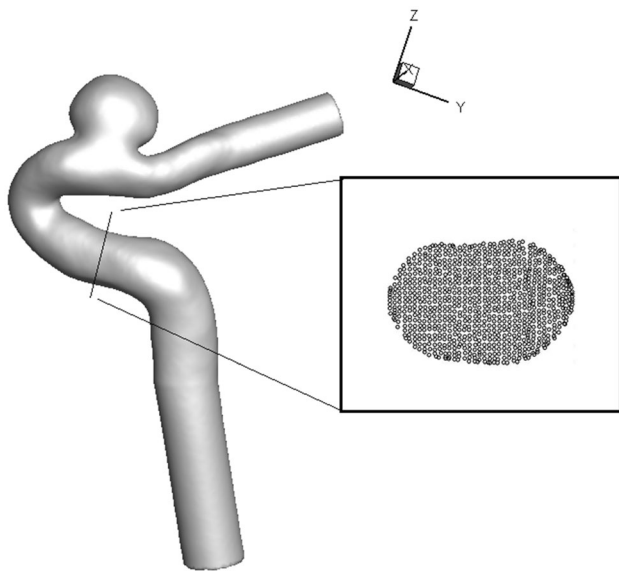


Fig. 3 Patient-specific geometry used in the study, inset shows the drug injection plane

particles when they pass through the 3D twist is also the focal point of the study.

2 Mathematical modeling

Blood is a complex fluid that exhibits different properties and behavior at different scales and pathological conditions. For the flow in cerebral arteries, blood cells have sufficiently small Stokes number to allow single-phase modeling with reasonable accuracy. Simulations are carried out using an unstructured three-dimensional Navier–

Stokes solver. The Eulerian–Lagrangian approach is used for this work. Fluid particle coupling is chosen to be one-way. The choice of particle size ($d = 50$ microns) also endorse this approach [6].

2.1 Governing equations and boundary conditions

Blood flow in the present work is treated as single-phase, incompressible and non-Newtonian. Equations (1), (2) and (3) are corresponding governing equations. A modified SIMPLE algorithm is used to solve these mass and momentum conservation equations. The targeted site also includes porous media. Porous media is modeled using Darcy–Brinkman–Forchheimer model [10]:

$$\nabla \cdot \mathbf{V} = 0 \tag{1}$$

$$\frac{\rho_f}{\varepsilon} \left[\frac{\partial \mathbf{V}}{\partial t} + \langle (\mathbf{V} \cdot \nabla) \mathbf{V} \rangle \right] = -\nabla \langle P \rangle^f + \frac{\mu}{\varepsilon} \nabla^2 \langle \mathbf{V} \rangle - \frac{\mu}{K} \langle \mathbf{V} \rangle - \frac{\rho_f F \varepsilon}{K^{0.5}} [\langle \mathbf{V} \rangle \cdot \langle \mathbf{V} \rangle] \mathbf{J} \tag{2}$$

As $\varepsilon = 1$ and $K \rightarrow \infty$ Eqs. 1 and 2 reduce to the Navier–Stokes equation. For porous media case porosity is taken as 0.735, permeability is $1.539\text{E} - 08 \text{ m}^2$ and the inertia coefficient is 0.2.

These equations are solved with no-slip boundary conditions for flow at the wall. While at inlet a physiological velocity waveform (Fig. 1) is used to give Womersley profile, Womersley profile is the fully developed velocity profile under periodic pulsatile flow conditions. Simulations are done for at least 10 cycles so that results obtained are free from any phase lag.

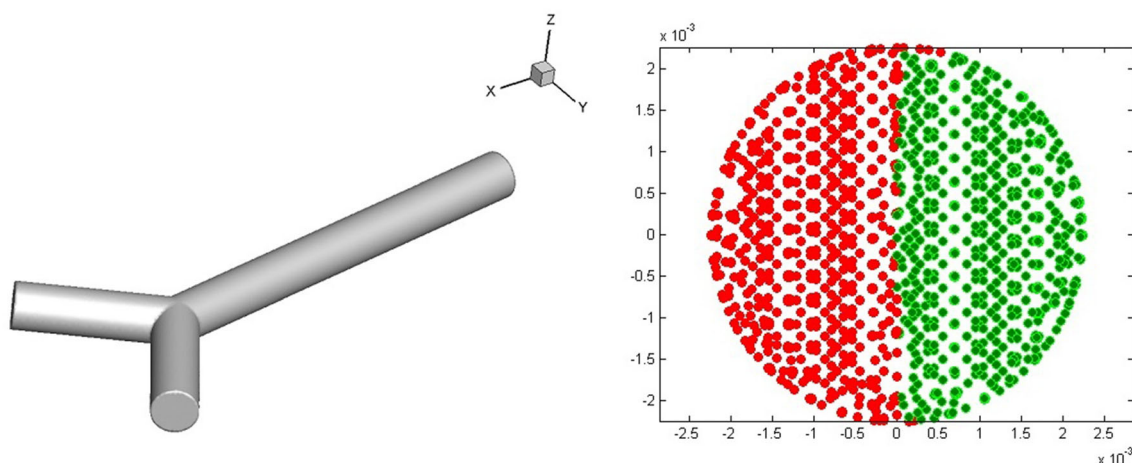


Fig. 4 Particle delivery through bifurcation of equally symmetric branches. Particle delivery map shows equivalence for both branches. Results are for $Re = 500$ and 1000 . Release location of particles flowing through same daughter branch vessel is shown with symbols of same color

Table 1 Case details

Case	Particle injection and aneurysm sac conditions
1	Tracer particle, particle diameter = $5E-05$ m, injection velocity = local flow
2	Particle density = 1500 kg/m^3 , particle diameter = $5E-05$ m, injection velocity = local flow
3	Particle density = 1500 kg/m^3 , particle diameter = $5E-05$ m, injection velocity = 0 m/s
4	Particle density = $10,000 \text{ kg/m}^3$, particle diameter = $5E-05$ m, injection velocity = local flow
5	Tracer particle, particle diameter = $5E-05$ m, injection velocity = local flow, porous sac
6	Particle density = 1500 kg/m^3 , particle diameter = $5E-05$ m, injection velocity = local flow, porous sac
7	Particle density = $10,000 \text{ kg/m}^3$, particle diameter = $5E-05$ m, injection velocity = local flow, porous sac
8	Particle density = 1500 kg/m^3 , particle diameter = $5E-05$ m, injection velocity = -0.3791 m/s. Injection velocity is set as constant. Injection velocity magnitude is chosen as the time average of inflow velocity waveform

2.2 Rheological model

Viscosity of blood can be taken as Newtonian for large arteries but for cerebral arteries with the sidewall aneurysm non-Newtonian modeling is required. Several generalized non-Newtonian models are available but the Carreau–

Yasuda model is preferred for modeling shear thinning behavior of blood. Work in [11] showed the stability and realistic prediction of the Carreau–Yasuda model [Eq. (3)] under all conditions.

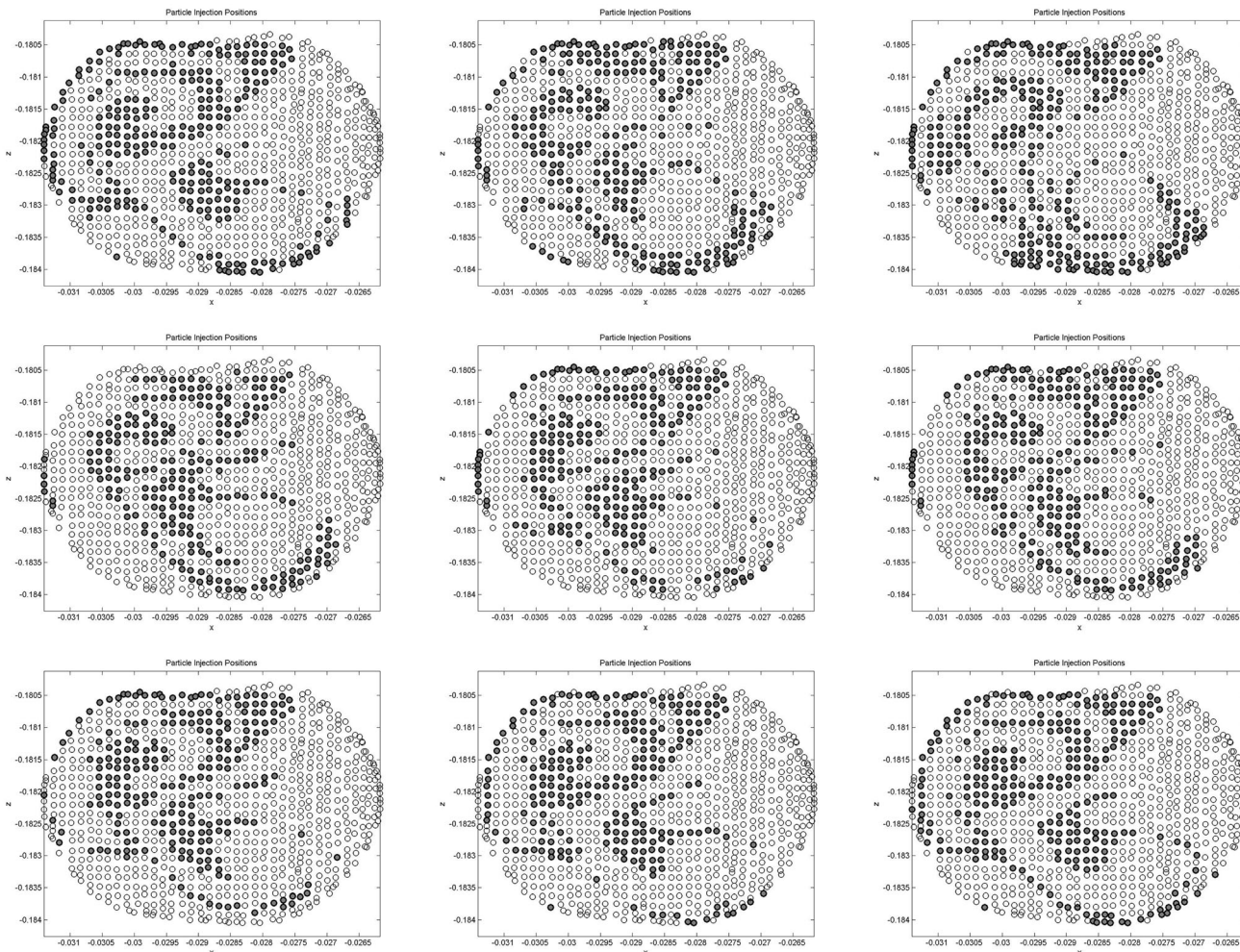


Fig. 5 DPRMs for case 1. First row (L-R): $t = 0.01, 0.11, 0.21$ (s); second row (L-R): $t = 0.31, 0.41, 0.51$ (s); third row (L-R): $t = 0.61, 0.71, 0.81$ (s)

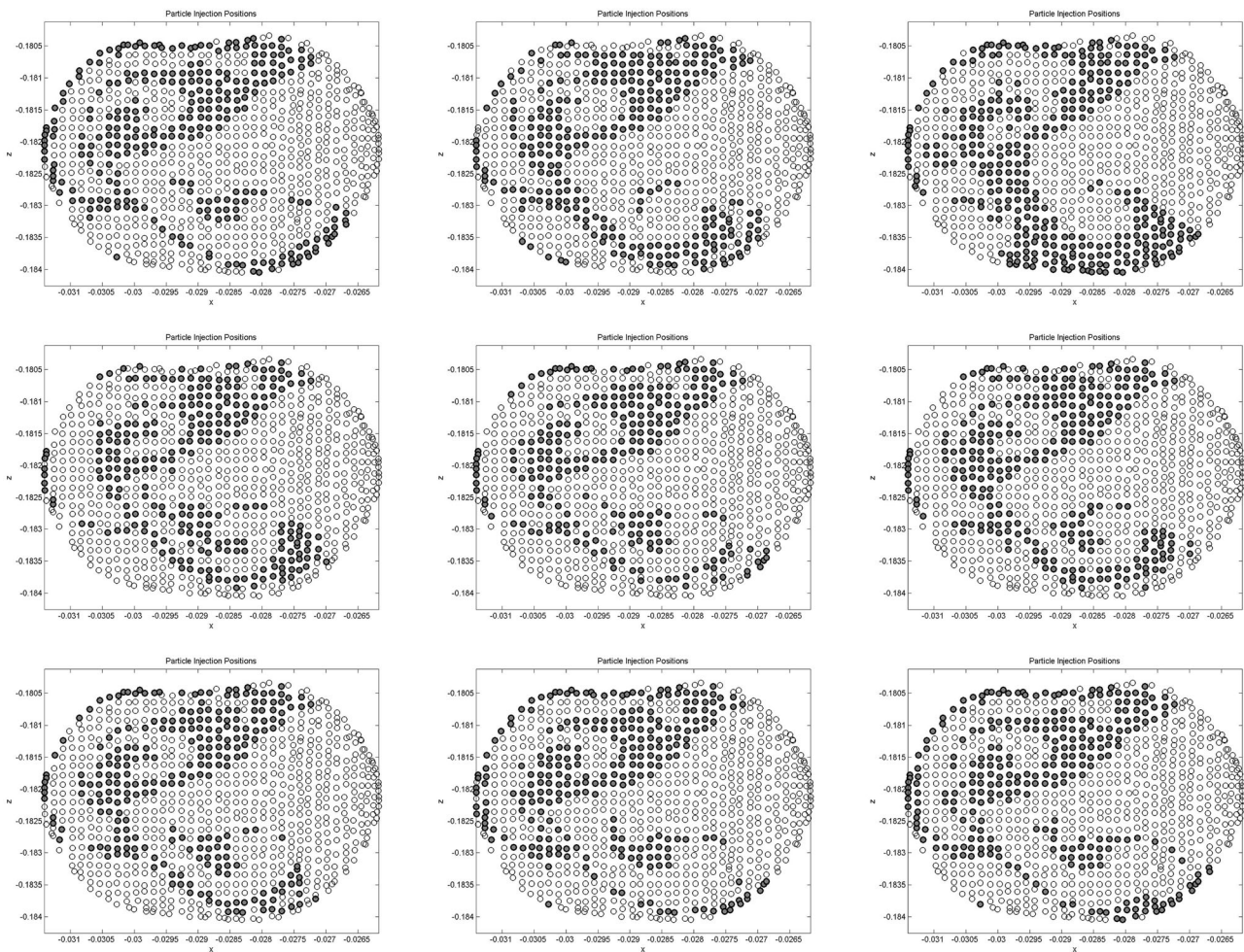


Fig. 6 DPRMs for case 2. First row (L-R): $t = 0.01, 0.11, 0.21$ (s); second row (L-R): $t = 0.31, 0.41, 0.51$ (s); third row (L-R): $t = 0.61, 0.71, 0.81$ (s)

$$\frac{\mu(\dot{\gamma}) - \mu_\infty}{\mu_0 - \mu_\infty} = [1 + (m\dot{\gamma})^n]^{-a}; \tag{3}$$

$$\dot{\gamma} = \left(\frac{1}{2}e_{ij}e_{ij}\right)^{1/2}; \quad e_{ij} = \frac{1}{2}\left(\frac{\partial u_i}{\partial x_j} + \frac{\partial u_j}{\partial x_i}\right)$$

where $\mu_0 = 1.6 \times 10^{-1}$ Pa s, $\mu_\infty = 3.5 \times 10^{-3}$ Pa s, $m = 8.2$ s, $n = 0.64$ and $a = 1.23$. The dynamic viscosity varies with the shear rate $\dot{\gamma}$ (calculated as the second invariant of the strain-rate tensor e_{ij}).

2.3 Particle transport

Particle transport simulation is carried out using a one-way coupling approach. As suggested in [1], virtual mass force, lift force, basset history forces are neglected. To assess the effect of arterial geometry only for heavy particle acceleration due to pressure gradient and gravity term is neglected, and only drag force is considered. In the

determination of DPRM, there is an inherent assumption that only one particle is released at a time. This minimizes the possibility of particle interaction. Thus, we neglected the particle–particle interaction. Infinite shear viscosity μ_∞ values are used for viscosity in particle transport calculations. A small-time step of size 10^{-4} s is used to get a smooth trajectory.

$$m_p \frac{dv_p}{dt} = \sum_i F_{P,i} \tag{4}$$

For the drag force coefficient Schiller–Naumann model [12] is used:

$$C_D = \frac{24}{Re} \left(1 + 0.15(Re)^{0.687}\right) \quad \text{For } Re < 1000$$

$$C_D = 0.44 \quad \text{For } Re \geq 1000 \tag{5}$$

$$Re = \frac{\rho_f d_p |V_p - V_f|}{\mu_f} \tag{6}$$

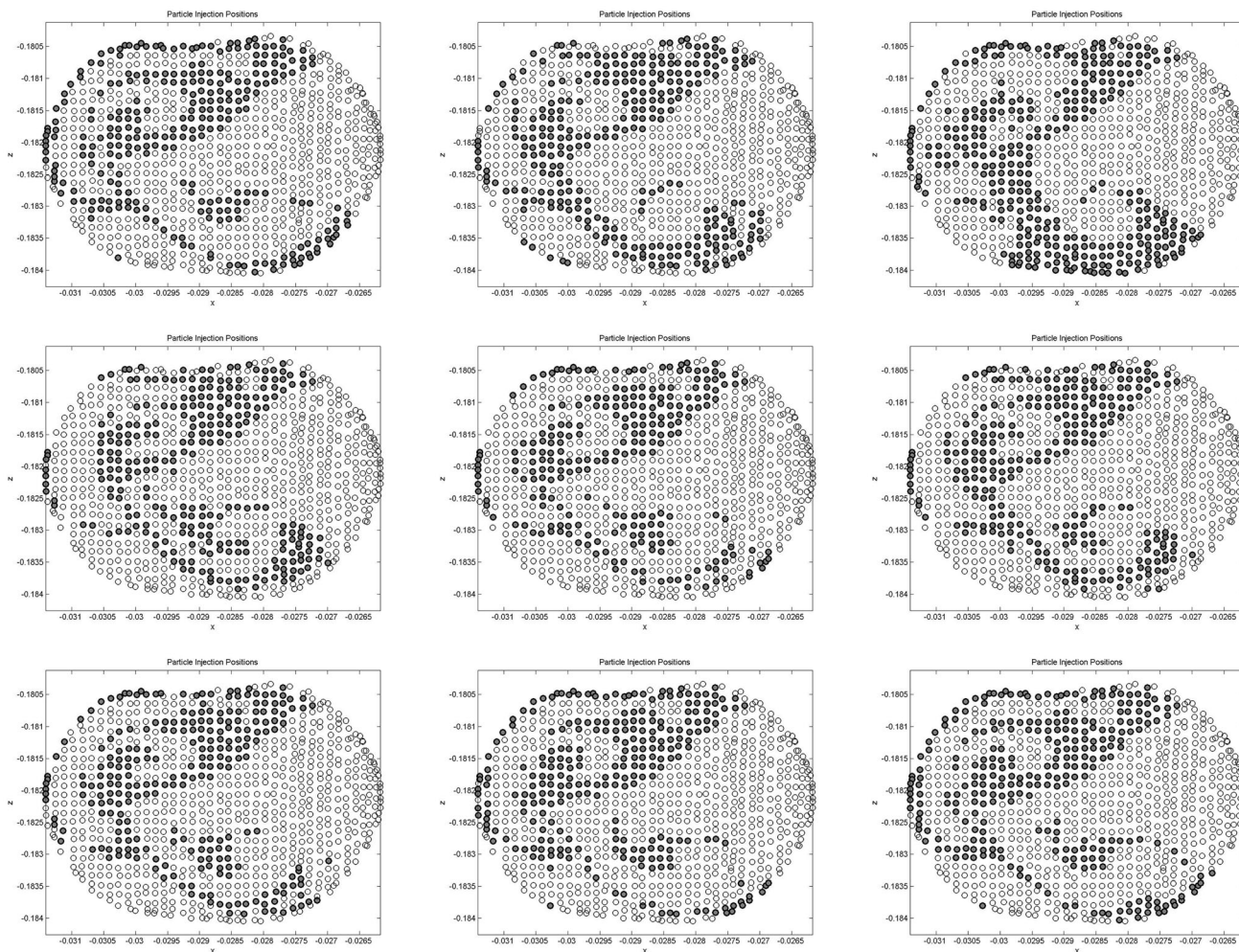


Fig. 7 DPRMs for case 3. First row (L-R): $t = 0.01, 0.11, 0.21$ (s); second row (L-R): $t = 0.31, 0.41, 0.51$ (s); third row (L-R): $t = 0.61, 0.71, 0.81$ (s)

2.4 Code validations

Simulations in the current work are carried out by an unstructured code that is well established, tested and validated. One of the validation is shown here for Womersley profile development in the straight tube for oscillatory flow. The velocity profile for different phase angles is shown and compared with the results of [13] in Fig. 2. A grid sensitivity study is done using a mesh size of 350,000, 480,000, 590,000 tetrahedron elements. Post-aneurysm lumen velocity is compared, and a maximum 2% deviation is observed for larger two meshes. Mesh size of 490,000 is used for the simulations. More validations including porous media are also shown in other publications [14, 15]. All particles are injected through a chosen plane, as shown in Fig. 3. The twist in the artery starts affecting the flow after the first bend and hence provides the realistic release conditions for the particles. Figure 4 shows the branch choice symmetry, with particle transport, for bifurcation

geometry. Results are checked for Reynolds number 500 and 1000.

2.5 Particle release strategy

Particles can be released at any location and at any time but will lead to significant systemic toxicity. Particle size, artery diameter, and targeted site environment put constraints on release conditions and timing. We explore four different release strategies (ensuring zero systemic toxicity) in this study. The first strategy is *Instantaneous Release*; in this, we release particles only at one selected time instant. The second strategy is *Complete Waveform Release*; in this, we release particles continuously over the complete waveform. The third strategy is *Systolic Release* and the fourth strategy is *diastolic release*; in these two cases, particles are released in systole and diastole part of the flow waveform respectively.

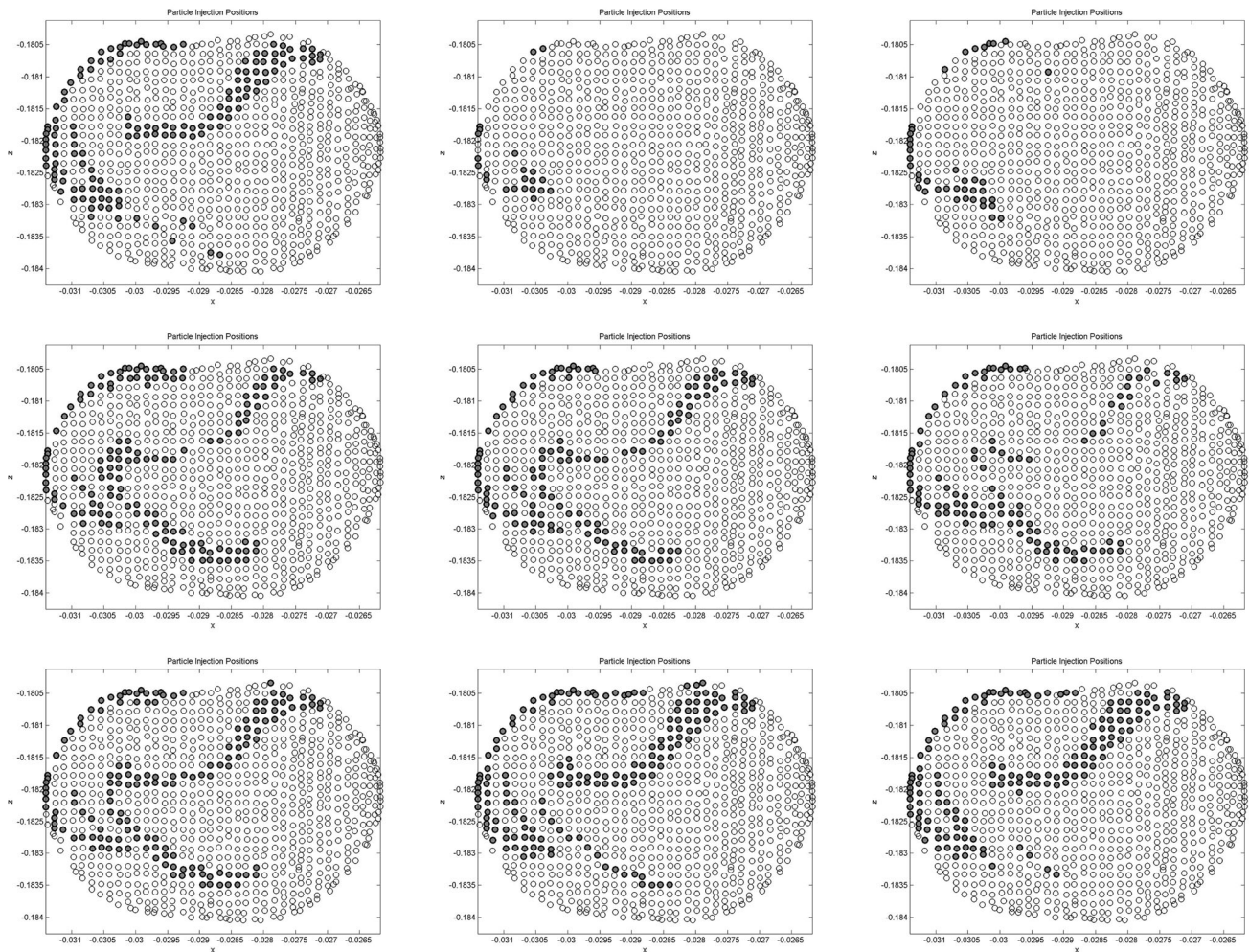


Fig. 8 DPRMs for case 4. First row (L-R): $t = 0.01, 0.11, 0.21$ (s); second row (L-R): $t = 0.31, 0.41, 0.51$ (s); third row (L-R): $t = 0.61, 0.71, 0.81$ (s)

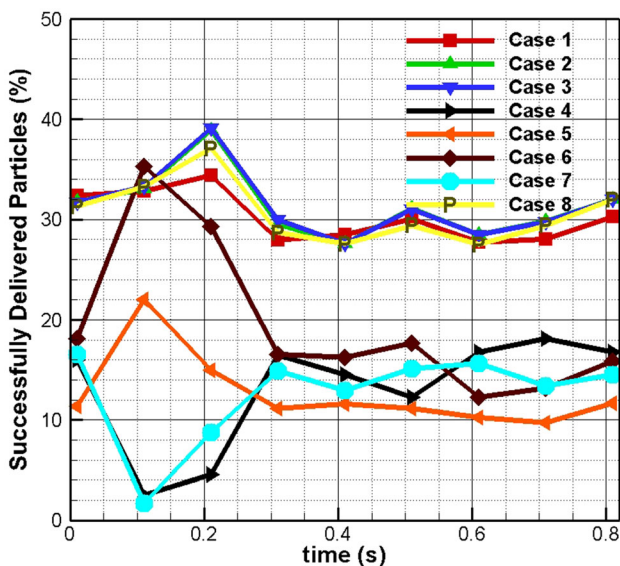


Fig. 9 Variation of particle delivery percentage with the flow waveform. Results are shown for all cases

2.6 Dynamic particle release map

Particles are injected through the chosen cross section (Fig. 3). Particles reaching inside aneurysm are deemed as successfully targeted, while plotting originating site of these particles are colored as black while rest are white. The contour forming of these successful delivery sites is DPRM. If a catheter is placed well within the DPRM, then systemic toxicity will become a minimum. Thus, assuming a circular opening of the catheter in-circle is found for the DPRMs and designated as an injection circle.

3 Results and discussion

The particle is injected uniformly from the injection plane. The first step of the investigation is to identify and characterize the injection locations from where particles surely

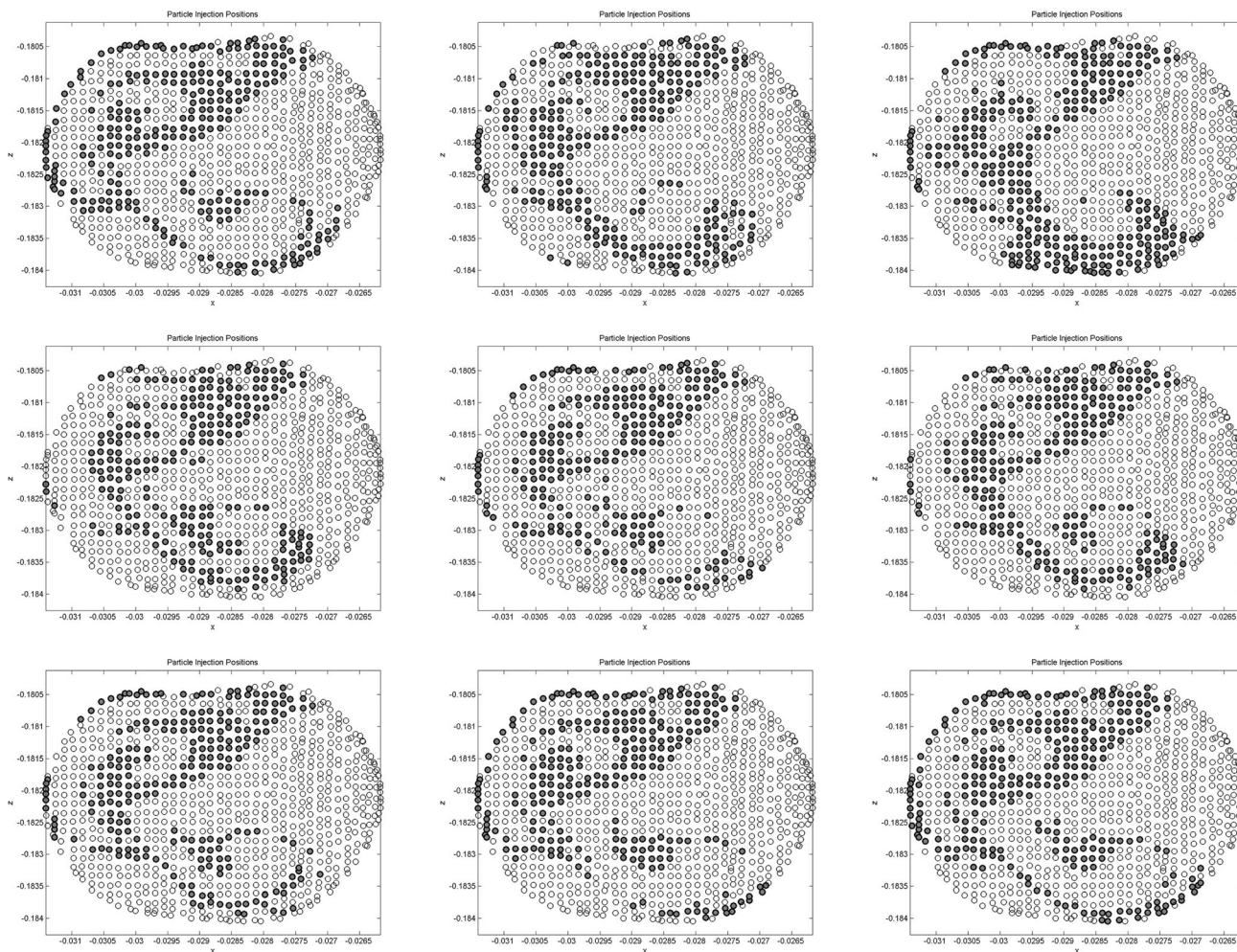


Fig. 10 DPRMs for case 8. First row (L-R): $t = 0.01, 0.11, 0.21$ (s); second row (L-R): $t = 0.31, 0.41, 0.51$ (s); third row (L-R): $t = 0.61, 0.71, 0.81$ (s)

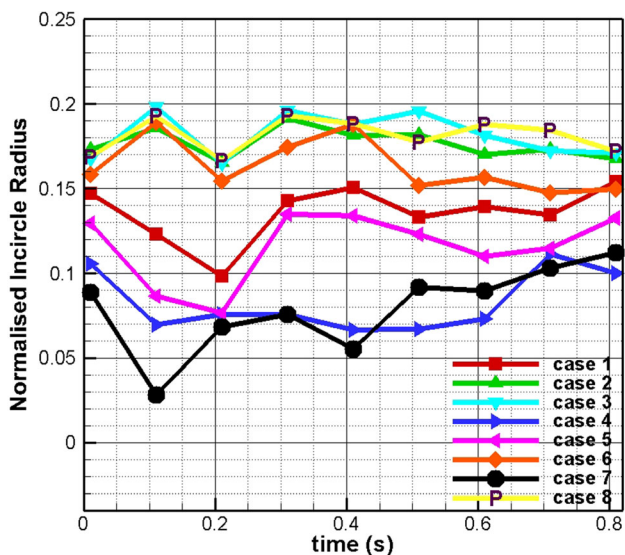


Fig. 11 Variation of normalized in-circle radius with the flow waveform. Results are shown for all cases

reach inside the aneurysm sac. A contour of all ensured delivery sites is being called a dynamic particle release map (DPRM). DPRM varies with the instantaneous Reynolds number. DPRMs reported in [2] appear to be much symmetric and ordered, while PRMs for the artery in the discussion is of very complex shape. This is due to the tortuous nature of the artery and location of the targeted aneurysm sac.

Temporally varying complex-shaped DPRMs complicates the site selection for catheter placement. The best approach to deal with the issue is to place a catheter at DPRM’s point at which the effects of temporal variation, vibrations and positioning error would be minimum. To determine such a safe location, we find the largest in-circle fitting inside the instantaneous PRM. The in-circle is the recommended site for catheter placement. These results are shown for 9 equally spaced time instants of flow waveform.

A particle starts from the chosen plane as shown in Fig. 3. The study involves two different kinds of particles

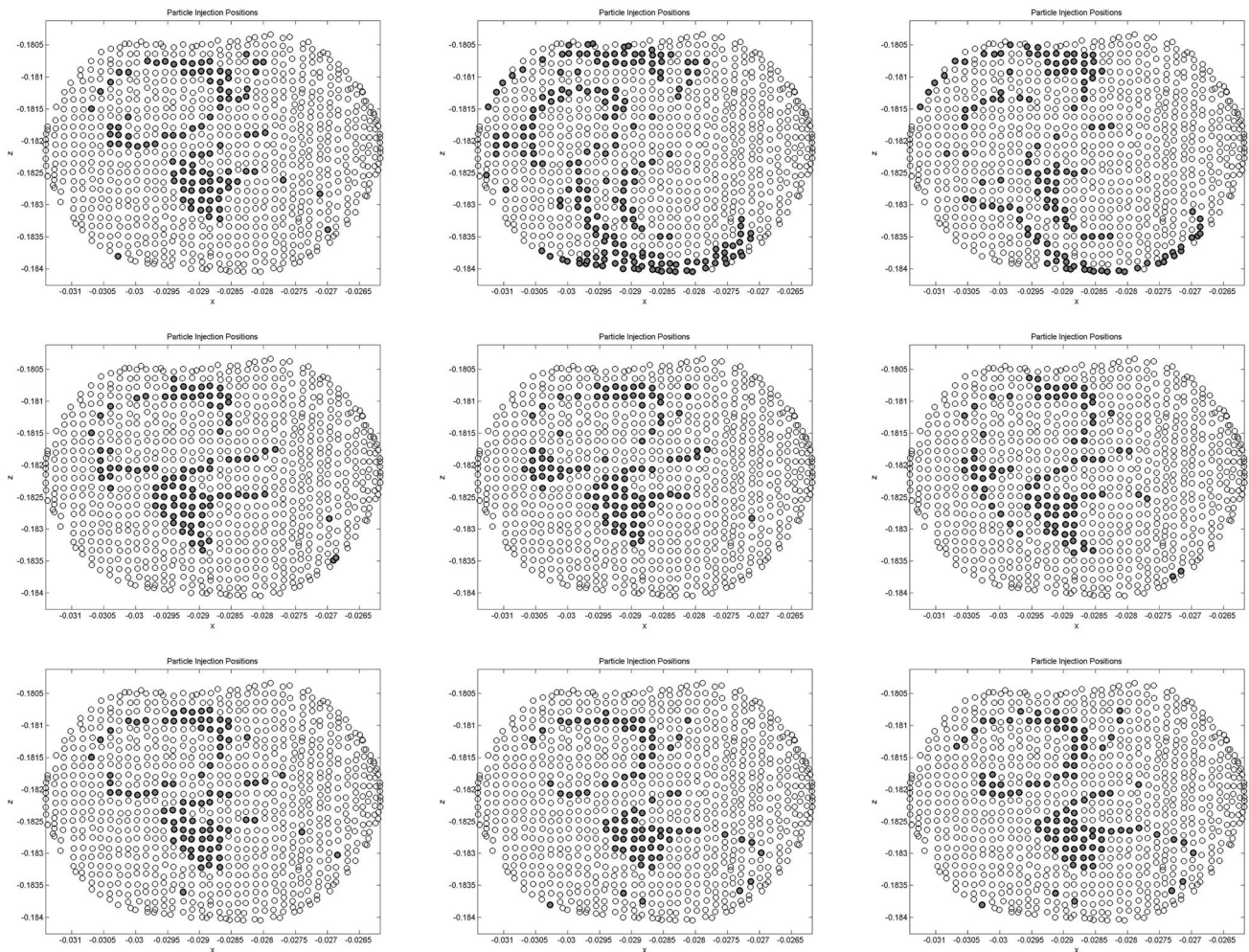


Fig. 12 DPRMs for case 5. First row (L-R): $t = 0.01, 0.11, 0.21$ (s); second row (L-R): $t = 0.31, 0.41, 0.51$ (s); third row (L-R): $t = 0.61, 0.71, 0.81$ (s)

with a similar size. First has no mass effect, i.e., being treated as a tracer particle, while the second type has mass effects. We use particles with two different densities. Table 1 lists the details of all eight cases. We calculate DPRM for nine equidistant time instants of flow waveform. Figure 5 shows the DPRM for case 1. Several patches of successful delivery sites appear where catheter could be placed. The variability of DPRMs restricts the choice of injection location. Careful examination of DPRMs reveals that DPRM is scattered and not symmetric compared to the results of [2] for planar arterial vasculature. Edge of successful delivery sites appears in curved shape. These curved contours shapes appear because of two different helical stream-bundles interacting with each other. The presence of bend and returning jet from the sac makes it more scattered.

Inertial effects exhibit differences in DPRMs in Figs. 6, 7 and 8 from DPRM in Fig. 5. The onset of inertial effects makes DPRMs less scattered thus increasing the possible

injection circle radius for heavy particles. Though comparing DPRMs of case 2 and 3 (Figs. 6, 7) with case 4 (Fig. 8) reveals that on further mass increase successful delivery sites decreases. Consecutively results in a decrease in the injection circle radius for very heavy particles. Though less frittered DPRM (Fig. 8) shows high inertial release locations. Differences in DPRMs of case 1 and case 2 & 3 is because of particle dispersion while differences in DPRMs of case 2 and 3 with case 4 arise because of anatomical reasons. Thus, while at the initial stage of density increase reduction in dispersion effect dominates while at the further increase geometrical complexities offset the reduction in dispersion effects. These effects can also be reconciled with the variation of successful delivery site percentage plot in Fig. 9. Dispersion and vasculature effects clearly manifest at the systole peak.

Case 8 has constant injection velocity for particles, chosen value is time average of inlet flow velocity waveform. Case 8 becomes relevant in practical conditions

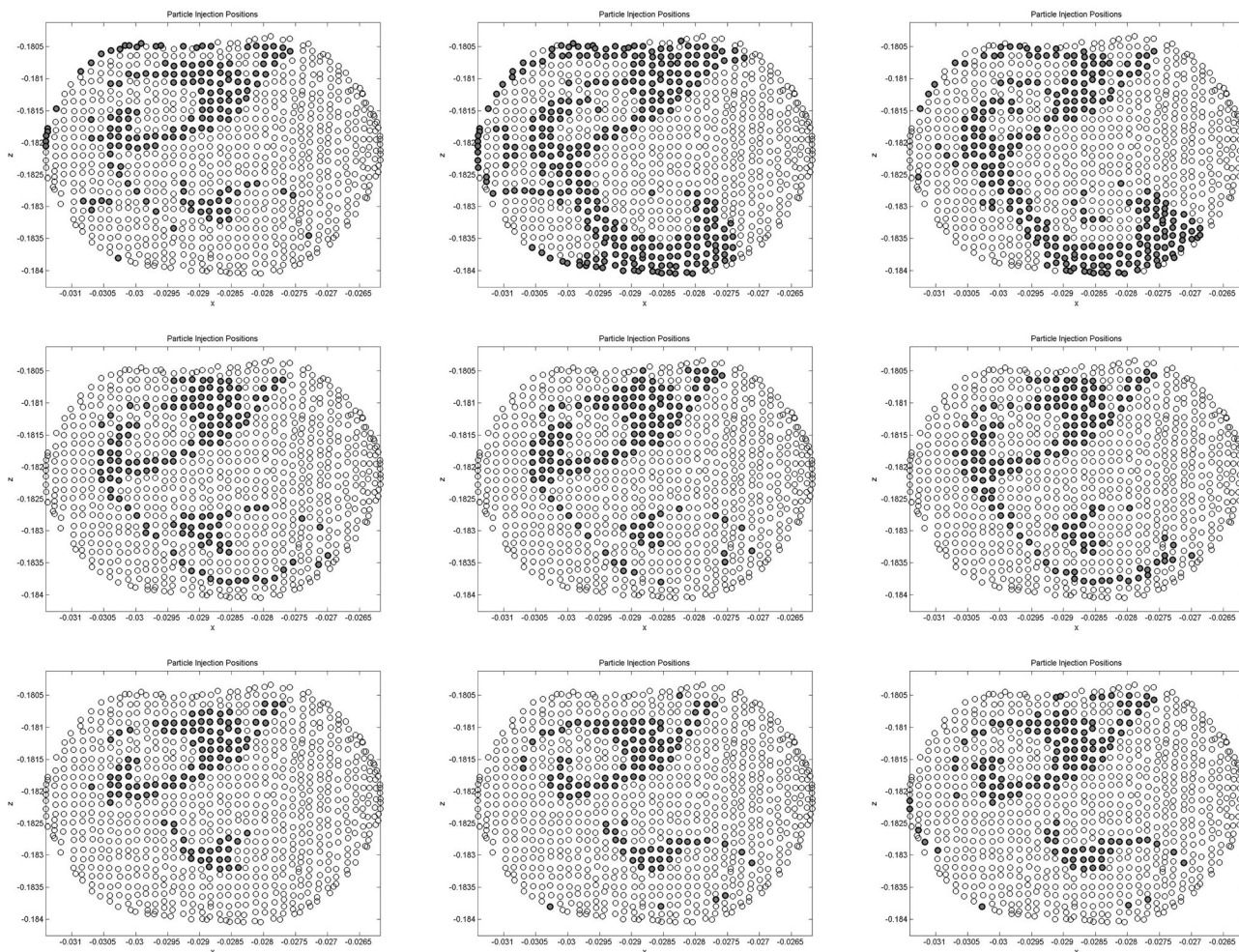


Fig. 13 DPRMs for case 6. First row (L-R): $t = 0.01, 0.11, 0.21$ (s); second row (L-R): $t = 0.31, 0.41, 0.51$ (s); third row (L-R): $t = 0.61, 0.71, 0.81$ (s)

where injection velocity is not the same as the local flow velocity. Comparison of cases 2, 3 and 8 (Figs. 6, 7, 10 respectively) reveals the effect of particle's injection velocity. Though because of small particle, consecutively high drag, no drastic changes are observed. Despite high drag, small differences appear in the diastolic phase of the waveform (Fig. 11).

Case 5, 6 and 7 investigate the effect of porous media presence in the targeted aneurysm sac. Figures 12, 13 and 14 compare their respective DPRMs. Compared to a clear aneurysm sac, a porous aneurysm sac filters the incoming flow. This reflects in respective DPRMs, successful delivery sites (Fig. 9) and injection circle radius. All three cases report more constrained conditions for targeted delivery compared to cases without a porous media presence. Comparison of DPRMs for tracer particles (in Figs. 5, 12) show significant changes. The presence of porous media creates a problem for lighter particles but for heavy particles, the situation does not change.

Figure 11 reports the variation of injection circle radius with time. Results are shown for all cases. As expected results are similar for cases 2, 3 and 8 in the systolic phase of flow waveform. Differences appear in the diastolic phase. These cases show variability of approximately 25% over the cycle for injection circle radius values. Results of the diastolic phase for cases 1, 2, 3 and 8 tend to converge to close values. This indicates the high predictability of targeted delivery in the sidewall aneurysm sac for the diastolic phase. The reduction in dispersion effects leads to an increase in the injection circle radius equivalent of 4% of the inlet radius. Case 2, 3, 6 and 8 show behavior in terms of injection circle radiation variation, systolic phase creates positive conditions for targeted delivery. Case 1 and 5 show similar variation along with case 5 and 8. Diastolic phase suits more for these cases for successful targeted delivery.

Figure 15 shows the injection circle's position, at nine different time instants, for all eight cases. The injection

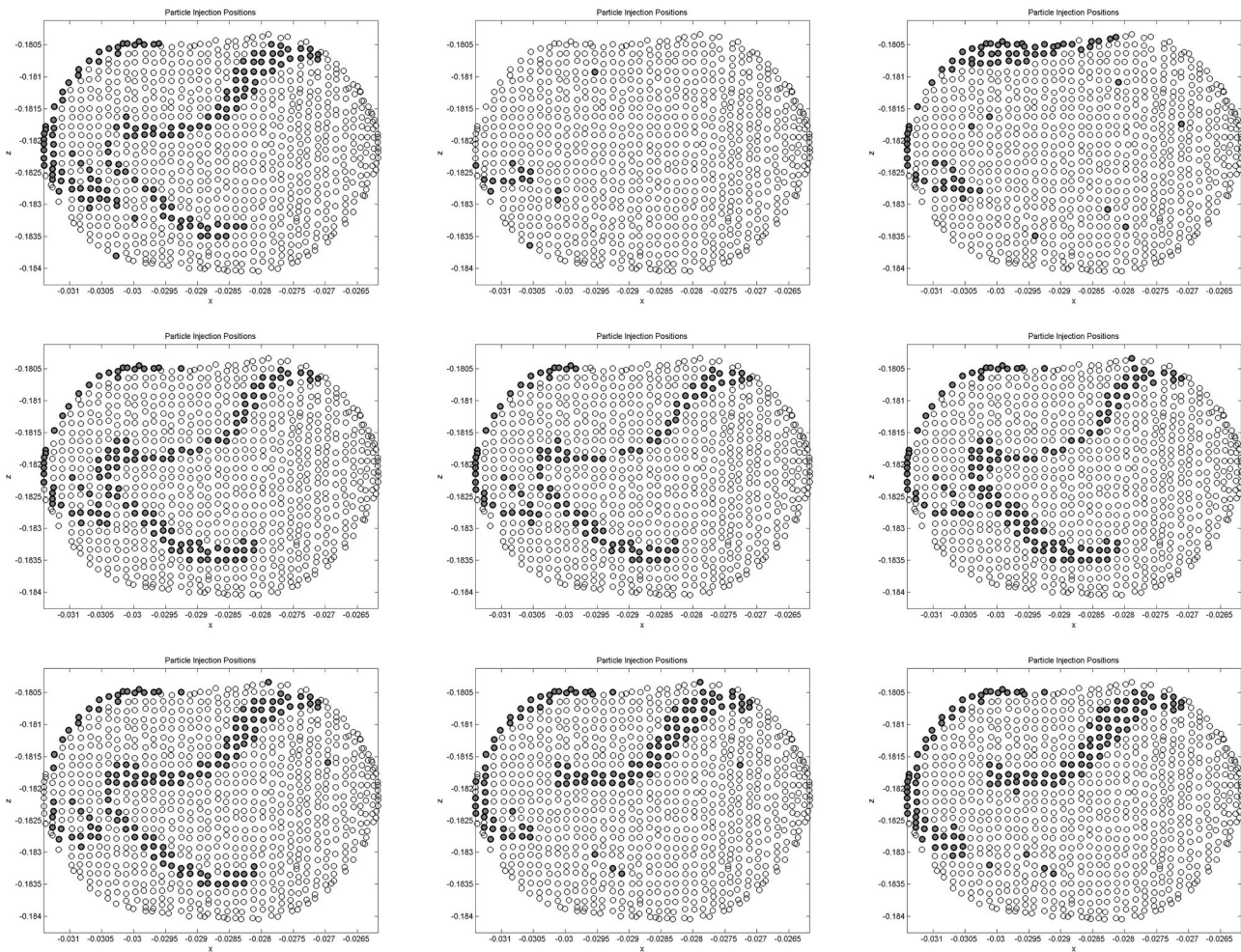


Fig. 14 DPRMs for case 7. First row (L-R): $t = 0.01, 0.11, 0.21$ (s); second row (L-R): $t = 0.31, 0.41, 0.51$ (s); third row (L-R): $t = 0.61, 0.71, 0.81$ (s)

circle's positional variation can also be clubbed for several cases. Case 1 and 5, for tracer particles, show very close injection circles. Case 2, 3 and 8 have their injection circles very close to each other for all time instants. Their size is also similar. Case 4 and 7 are similar. Instantaneous acceleration tends to create a distinction between cases in similar clubs. Higher the acceleration at the time of particle release farther would be the injection circles' for different cases in a similar club. Though injection circle for tracer act contrary to this logic, which can be attributed to two similar-sized patches of DPRMs.

Figure 16 shows the time-lapse plot of injection circles for all eight cases. Results show that injection circles scatter at the systolic peak. For very high-density cases (4 and 7) a clear distinction between the injection circle of the systolic phase and the diastolic phase can be seen.

Variability of injection circle's position and size, with different instantaneous Reynolds number, particle release conditions, and target environment, mandates continuous

shifting of catheter position to ensure the least systemic toxicity for uniform release. Continuous shifting of the catheter isn't a viable option due to practical reasons. Thus, we calculate DPRMs for the whole waveform which consists of release sites ensuring 100% successful delivery for the full waveform. Considering the effects of systolic and diastolic phases we repeated this exercise for systolic and diastolic part of the waveform. Corresponding DPRMs are shown in Fig. 17.

Continuous release over the full waveform severely restricts the largest possible catheter size for zero systemic toxicity. Figures 18, 19 and 20 show the largest in-circle or injection (in case of zero safety margin) circle radius for systolic, diastolic phase and full waveform, respectively. Figures 21, 22 and 23 reports the percentage of successful release sites for each case. Depending on the availability of catheter size different release patterns could be adopted. Releasing at systole peak allows the largest catheter size for cases 2, 3, 6 and 8 while release at diastole minima

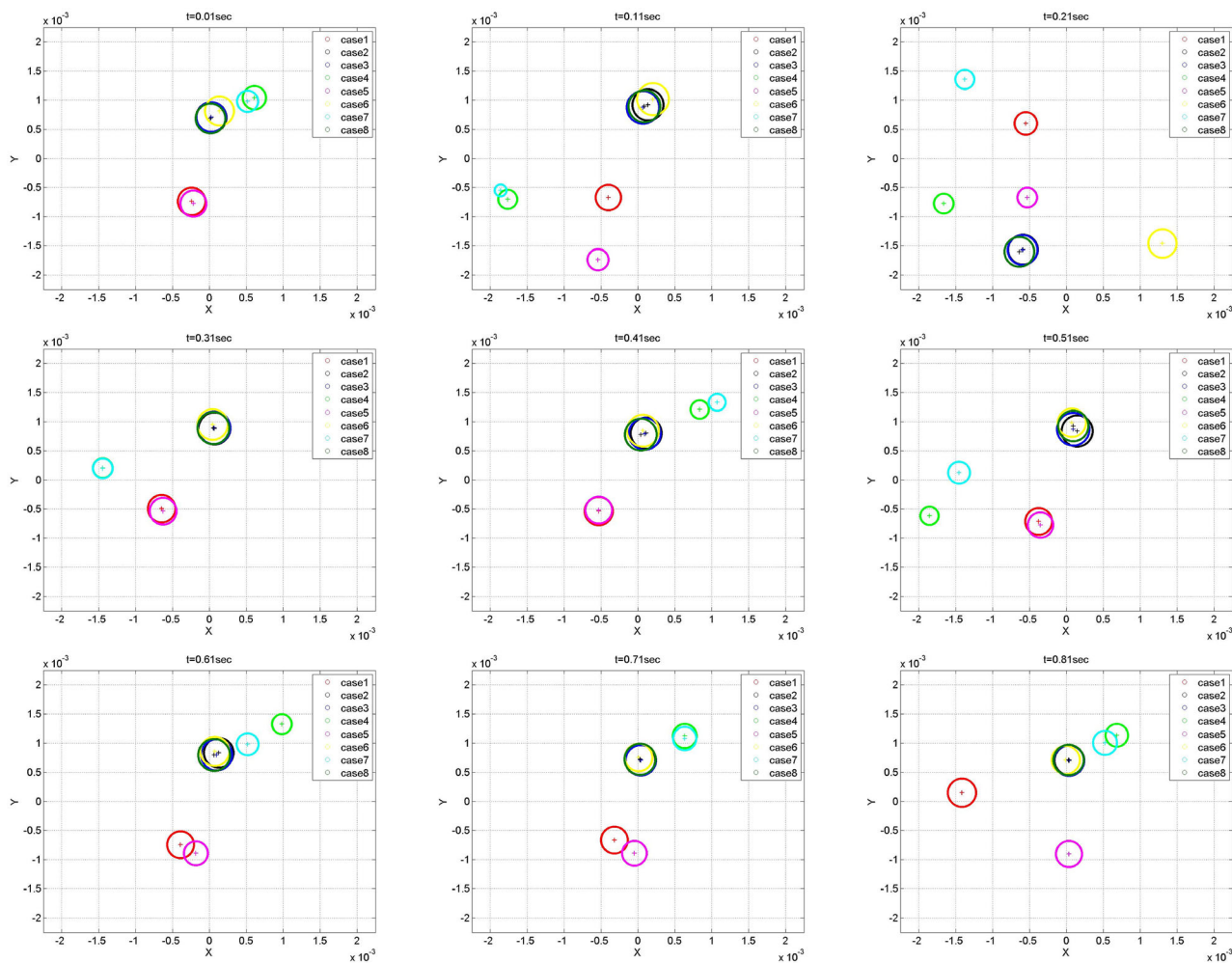


Fig. 15 In-circles of all eight cases plotted for nine different, equally spaced, time instants over the waveform

allows the largest catheter size for the rest of the cases. Though large particles mandate the strategy of releasing once in full-cycle it leads to large intrusion time period. Large intrusion can further lead to hemodynamic complications thus should be avoided. The best approach would be to release particles only in the diastolic phase which offer a significant reduction in catheter intrusion time and simultaneously significant particle size compared to systole release, full waveform release.

4 Conclusions

The study is carried out to analyze targeted particle delivery, injected from a predetermined plane, inside an aneurysm sac. The dynamic particle release map (DPRM) for optimal delivery is generated and analyzed. Results are compared for three different kinds of particles, two with moderate density and large density and one without mass effects. The maximum possible catheter size is determined using four different particle injection strategy. Important aspects of the study and main conclusions are as following:

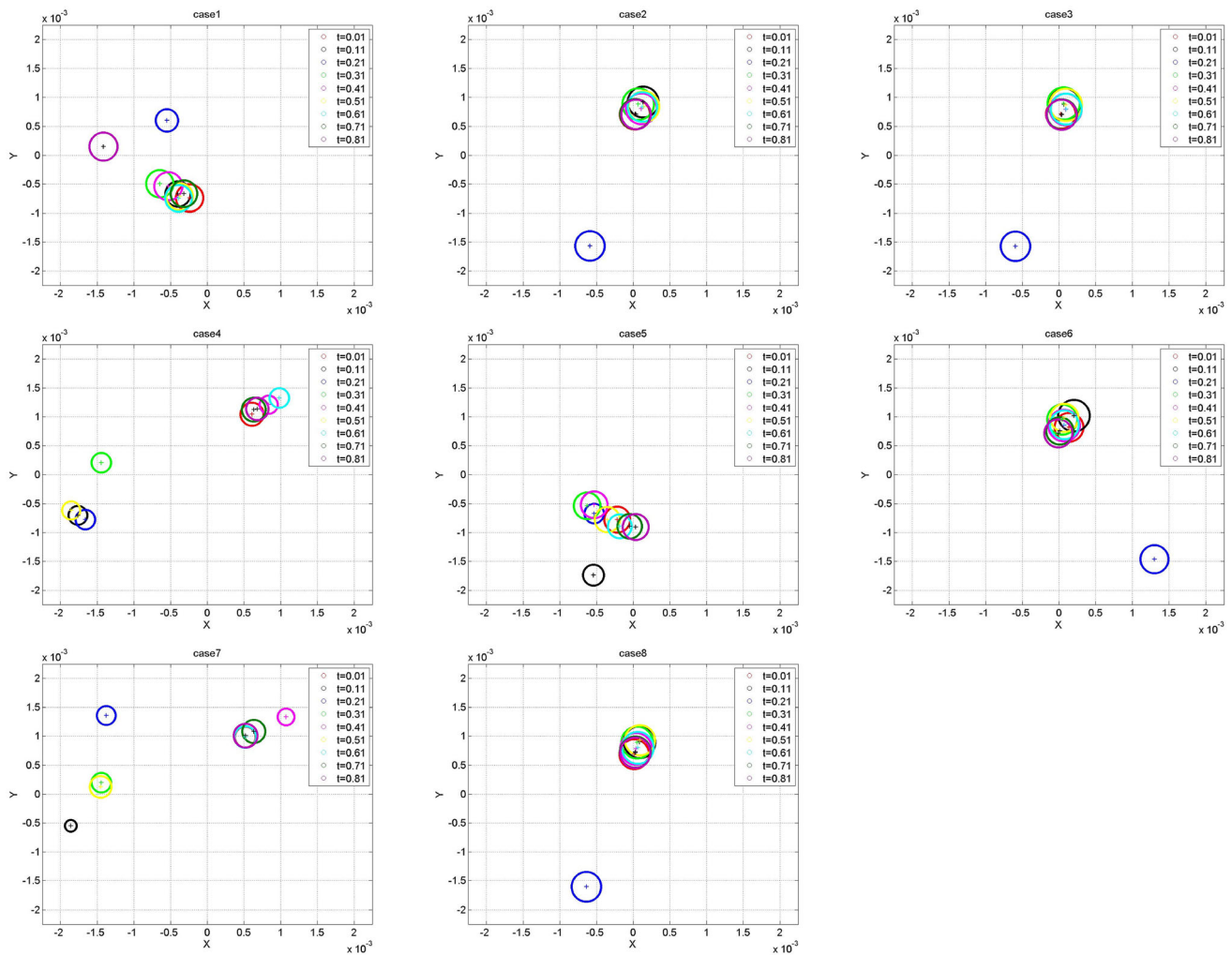


Fig. 16 In-circles of all nine different time instants plotted separately for each case

- (a) The strategy for optimal positioning of the catheter is proposed. Different release strategy permits different maximum catheter size. In order of decreasing maximum permissible catheter size release strategies are single instant release, diastole release, systole release then with least catheter diameter the complete waveform release strategy. For large density particles or large catheter sizes, an instantaneous release strategy should be employed. In the case of large uncertainty and less intrusion time available, the diastole release strategy should be opted.
- (b) Injection circle radius size and location both differ significantly (Fig. 15) for tracer particles and heavy particles. Though the moderate density particles permit double catheter diameter than tracer particles but the location of the injection circle shift significantly ($\sim 35\%$ of artery diameter). Thus, the use of tracer particles for determining the PRM can lead to significant error.
- (c) The effect of dispersion, inertia, and vasculature induced flow complexities compete with each other to determine the DPRMs. Inertia dominated effects are

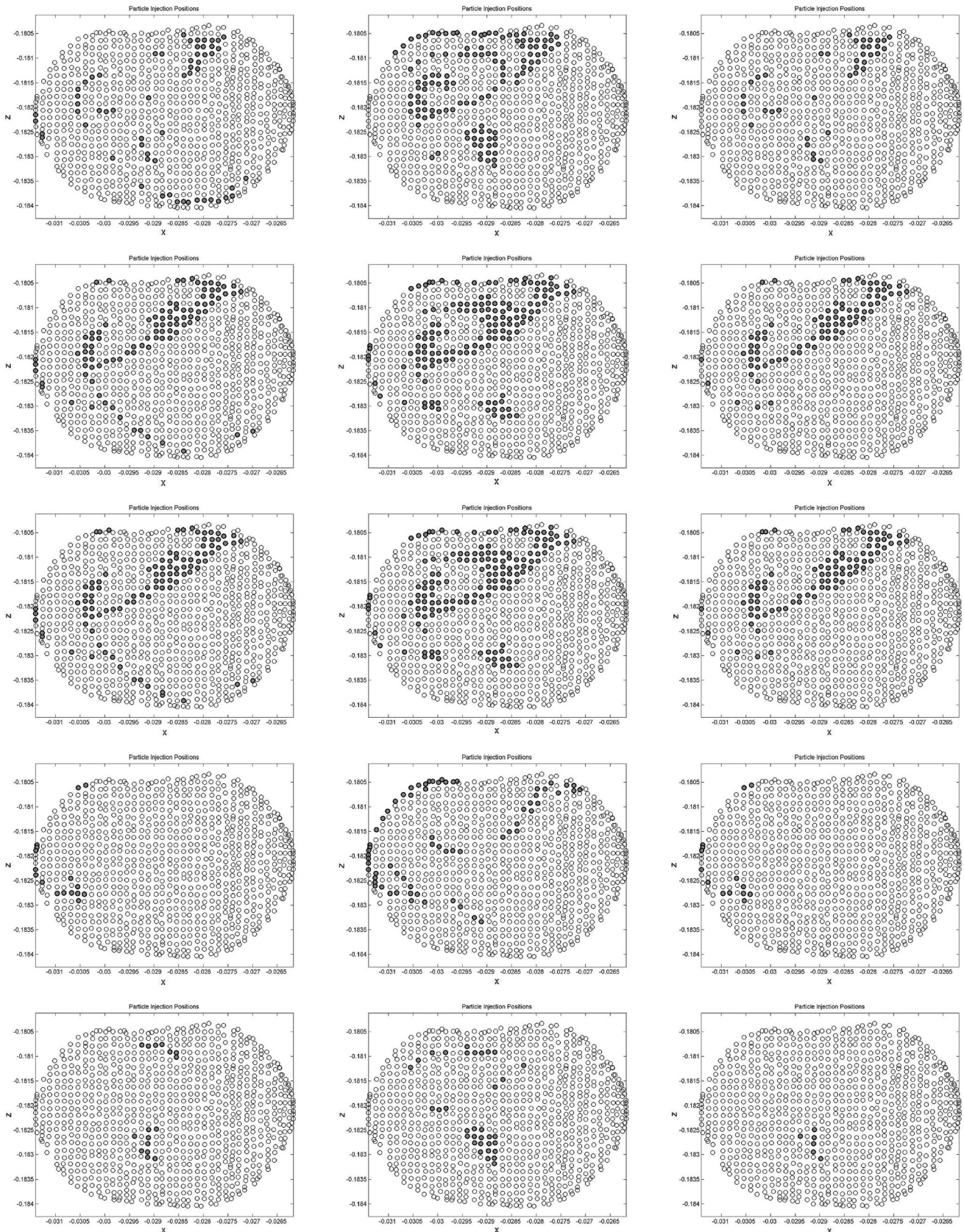


Fig. 17 DPRMs for cases 1 to 8 (row-wise). Systole (First Column), Diastole (Second Column) and full Waveform (Third Column) release strategy based DPRMs are shown for comparison

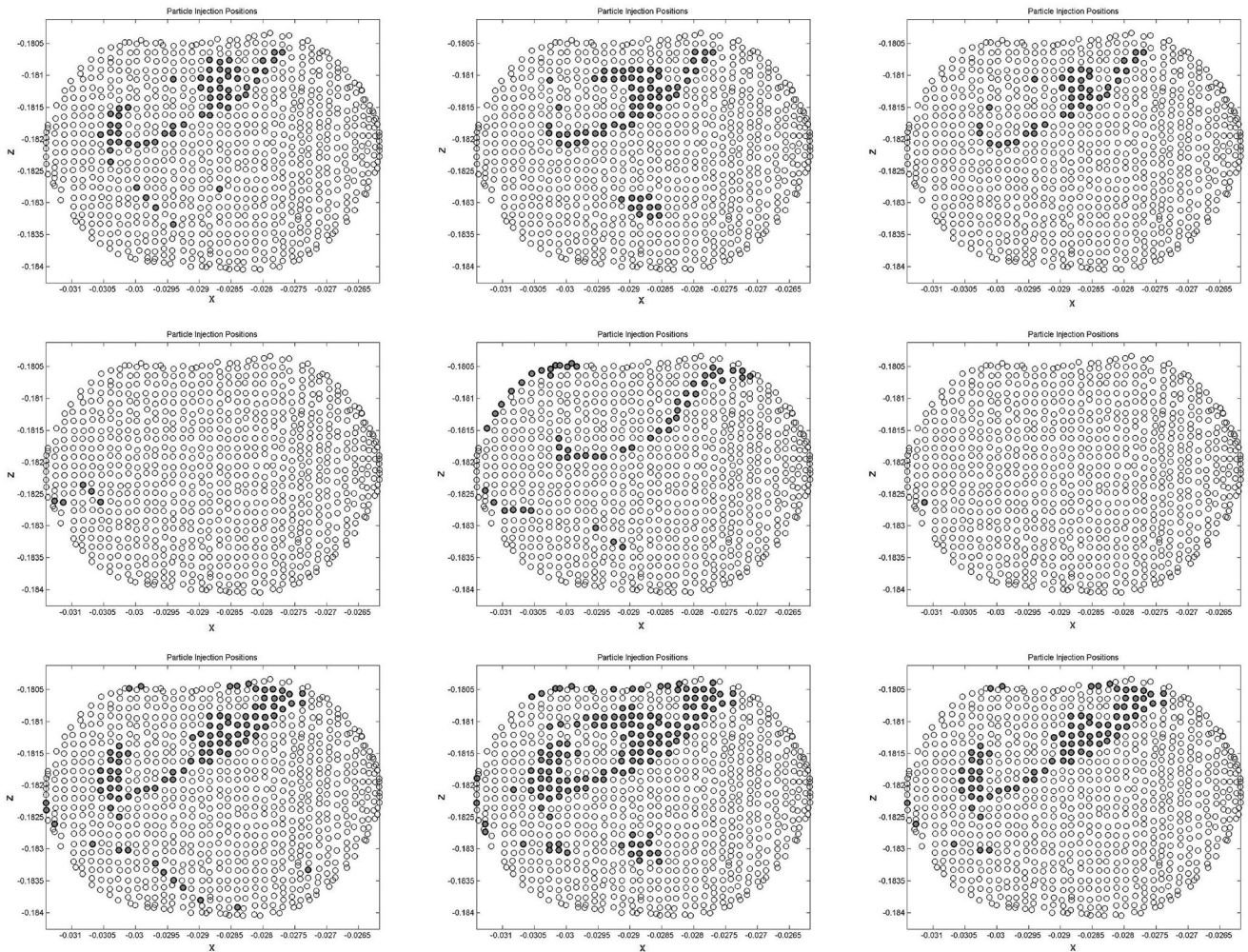


Fig. 17 continued

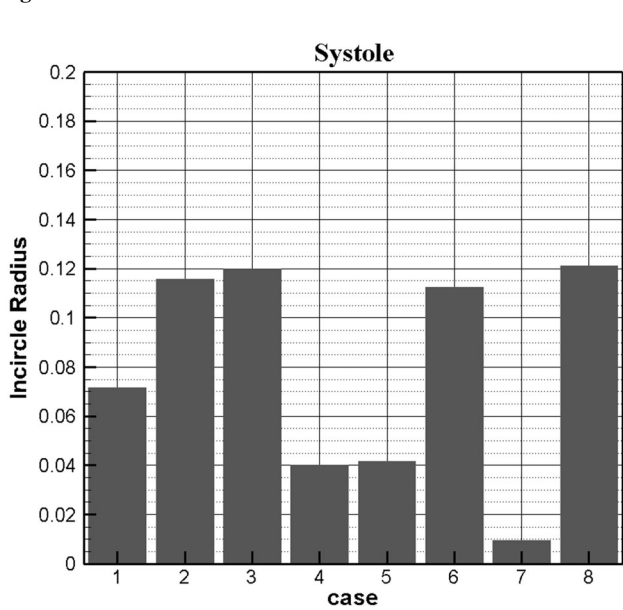


Fig. 18 Incircle or injection circle radius (normalized) for systole release strategy

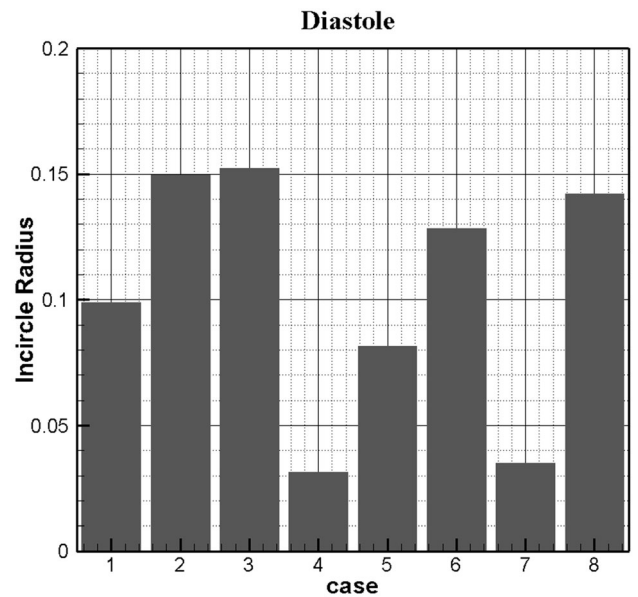


Fig. 19 Incircle or injection circle radius (normalized) for diastole release strategy

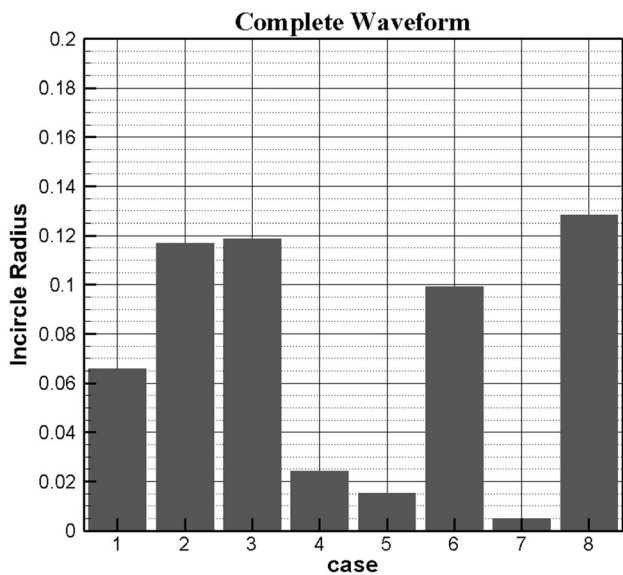


Fig. 20 Incircle or injection circle radius (normalized) for complete waveform release strategy

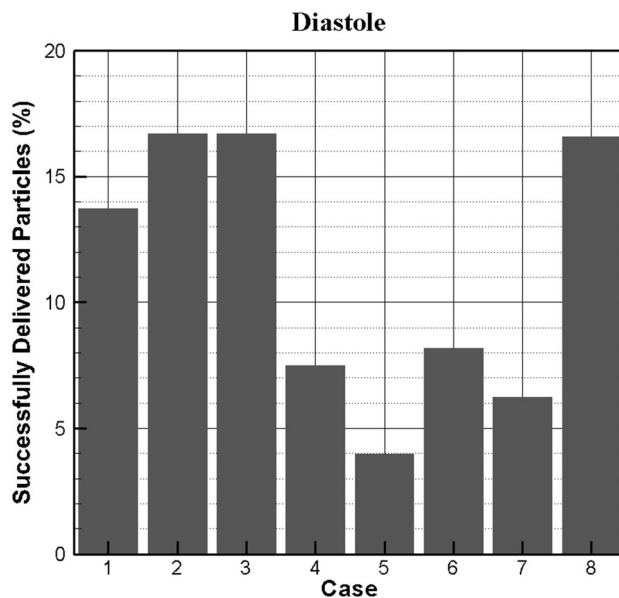


Fig. 22 Successfully delivered particle percentage for diastole release strategy

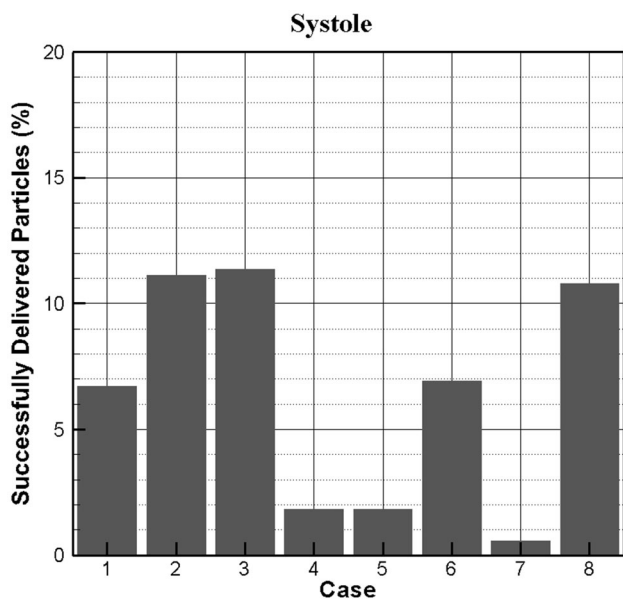


Fig. 21 Successfully delivered particle percentage for systole release strategy

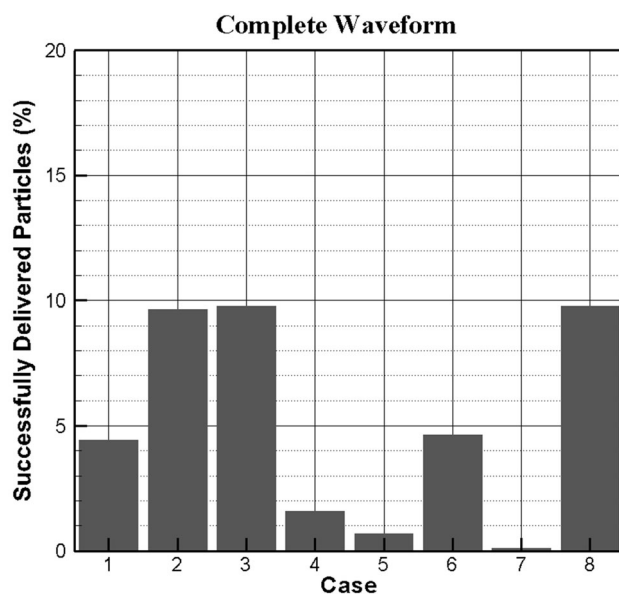


Fig. 23 Successfully delivered particle percentage for complete waveform release strategy

seen for heavier particles, a safe region for catheter injection reduces significantly. High-density particles can more easily target the porous aneurysm sac as similar to sac without porous media.

- (d) For tracer and light particles injection circle remains consistently at one position except at the systole peak. For very heavy particle injection circles form at two different regions depending on the systolic and

diastolic phase. Thus, for heavy particles complete waveform release should be strictly avoided.

Acknowledgements We gratefully acknowledge the computing facilities provided by the Indian Institute of Technology Kanpur.

References

1. Basciano, C.A., Kleinstreuer, C., Kennedy, A.S., Dezar, W.A., Childress, E.: Computer modeling of controlled microsphere release and targeting in a representative hepatic artery system. *Ann. Biomed. Eng.* **38**(5), 1862–1879 (2010)
2. Childress, E.M., Kleinstreuer, C.: Computationally efficient particle release map determination for direct tumor-targeting in a representative hepatic artery system. *J. Biomech. Eng.* **136**(1), 011012 (2013)
3. Fuchs, K., Duran, R., Denys, A., Bize, P.E., Borchard, G., Jordan, O.: Drug-eluting embolic microspheres for local drug delivery—state of the art. *J. Control. Release* **262**(April), 127–138 (2017)
4. Popel, A.S., Johnson, P.C.: Microcirculation and hemorheology. *Annu. Rev. Fluid Mech.* **37**, 43–69 (2005)
5. Bushi, D., Grad, Y., Einav, S., Yodfat, O., Nishri, B., Tanne, D.: Hemodynamic evaluation of embolic trajectory in an arterial bifurcation: an in-vitro experimental model. *Stroke* **36**(12), 2696–2700 (2005)
6. Mukherjee, D., Padilla, J., Shadden, S.C.: Numerical investigation of fluid–particle interactions for embolic stroke. *Theor. Comput. Fluid Dyn.* **30**(1–2), 23–39 (2016)
7. Carr, I.A., Nemoto, N., Schwartz, R.S., Shadden, S.C.: Size-dependent predilections of cardiogenic embolic transport. *AJP Heart Circ. Physiol.* **305**(5), H732–H739 (2013)
8. Ta, H.T., Truong, N.P., Whittaker, A.K., Davis, T.P., Peter, K.: The effects of particle size, shape, density and flow characteristics on particle margination to vascular walls in cardiovascular diseases. *Expert Opin. Drug Deliv.* **15**(1), 33–45 (2018)
9. Fabbri, D., Long, Q., Das, S., Pinelli, M.: Computational modelling of emboli travel trajectories in cerebral arteries: influence of microembolic particle size and density. *Biomech. Model. Mechanobiol.* **13**(2), 289–302 (2014)
10. Khanafer, K.M., Gadhoke, P., Berguer, R., Bull, J.L.: Modeling pulsatile flow in aortic aneurysms: effect of non-Newtonian properties of blood. *Biorheology* **43**(5), 661–679 (2006)
11. Kim, Y.H., VandeVord, P.J., Lee, J.S.: Multiphase non-Newtonian effects on pulsatile hemodynamics in a coronary artery. *Int. J. Numer. Methods Fluids* **58**, 803–825 (2008)
12. Gidaspow, D.: *Multiphase Flow and Fluidization: Continuum and Kinetic Theory Descriptions*. Academic press, Cambridge (2012)
13. Timité, B., Castelain, C., Peerhossaini, H.: Pulsatile viscous flow in a curved pipe: effects of pulsation on the development of secondary flow. *Int. J. Heat Fluid Flow* **31**(5), 879–896 (2010)
14. Paul, C., Das, M.K., Muralidhar, K.: Three-dimensional simulation of pulsatile flow through a porous bulge. *Transp. Porous Media* **107**, 843–870 (2015)
15. Pandey, P.K., Das, M.K.: Study of targeted particle delivery in the cerebral aneurysm. In: 7th International and 45th National Conference on Fluid Mechanics and Fluid Power (FMFP) (2018)

Publisher's Note

Springer Nature remains neutral with regard to jurisdictional claims in published maps and institutional affiliations.